Journal of Environmental Chemical Engineering 4 (2016) 516–526

Contents lists available at ScienceDirect

Journal of Environmental Chemical Engineering

journal homepage: www.elsevier.com/locate/jece

Application of soy hull biomass in removal of Cr(VI) from contaminated waters. Kinetic, thermodynamic and continuous sorption studies

Patricia S. Blanes[a,b], María E. Bordoni[a], Juan C. González[a,b], Silvia I. García[a,b], Ana M. Atria[c], Luis F. Sala[a,b], Sebastián E. Bellú[a,b,*]

[a] Área Química General, Departamento de Químico-Física, Facultad de Ciencias Bioquímicas y Farmacéuticas, Universidad Nacional de Rosario, Suipacha 531, S2002LRK Rosario, Santa Fe, Argentina
[b] Instituto de Química de Rosario-CONICET, Suipacha 570, S2002LRK Rosario, Santa Fe, Argentina
[c] Facultad de Ciencias Químicas y Farmacéuticas-Universidad de Chile, Olivos 1007, Santiago, Región Metropolitana, Chile

ARTICLE INFO

Article history:
Received 9 September 2015
Received in revised form 6 November 2015
Accepted 4 December 2015
Available online 8 December 2015

Keywords:
Chromium
Soy hull
Kinetics
Thermodynamics
Biosorption

ABSTRACT

Soy hull was evaluated as a new material for Cr(VI) removal from aqueous solutions. Cr(VI) removal was associated to a redox mechanism, in which Cr(VI) was reduced to Cr(III) by the biomass. The redox capacity of soy hull was 1.12 mmol g^{-1}. A kinetic model that considers the redox reaction between Cr(VI) and the biomass surface was proposed. The maximum sorption capacity was 7.286 mg g^{-1} at 20 °C and pH 1.5. Activation parameters and mean free energies suggest that the sorption process follows a mechanism of chemical sorption. Thermodynamic parameters show that Cr(VI) removal was spontaneous. The isosteric heat of sorption indicated that soy hull has an energetically homogeneous surface. XPS spectra showed that chromium bound on the biomass was Cr(III). These results were confirmed by XANES and EXAFS experiments. EPR spectra showed the presence of Cr(V)-soy hull at short contact time and only a signal corresponding to Cr(III)-soy hull at long contact times. Continuous sorption data were fitted to Thomas and modified dose–response models. The bed depth service time (BDST) model was used to scale-up the continuous sorption experiments.

1. Introduction

Chromium is a very toxic heavy metal, and it is discharged in the effluents from many industries, including steel plants, electroplating, tannery, and pigment and dye industries [1]. Most chromium exists in the environment as Cr(VI) and Cr(III). Compared with Cr(III), Cr(VI) is a highly toxic heavy metal, which is able to cause cancer in humans and animals, thus it has been designated as one of the top-priority toxic pollutants by the U.S. EPA. The allowed limit given by US EPA for Cr discharged is 0.1 mg L^{-1} [2]. Besides, Cr(III) is susceptible to precipitation in soil strata while Cr(VI) is mobile and always leached out by groundwater. Thus, removal of Cr(VI) from wastewater or soil to avoid Cr pollution is a key step when designing environmental friendly processes [3].

Many different types of treatment processes have been used successfully to remove hexavalent chromium from polluted effluents, including ion exchange [4], chemical reduction [5], activated carbon [6], chemical absorption [7], membranes [8], and electrochemical processes [9]. Compared to other methods, sorption is one of the most popular and cost-efficient methods, and can be used for recovering Cr(VI) at low concentrations [10]. Many different materials have demonstrated their capacity to remove chromium, including carrot residues [11], eggshells [12], coir pitch [13], rice husk and citric peels [14], sawdust [15], activated neem bark [16]. To effectively apply these materials in sorption removal processes of heavy metals, it is essential to determine the parameters that affect metal sorption.

Soy is one of the major agricultural products in the world. Argentina stands as the third largest producer of soybeans, accounting for 18% of the world production. The oil and protein constituents of soybeans are the main products in soy cultivation while the hulls are usually discarded [17]. Soy hull is a by-product of the soybean oil industry. For each ton of soy seed processed, about 2% of the total mass corresponds to this by-product [18]. Soy hulls constitute about 8% of the whole seed and contain about 86% complex carbohydrates. The insoluble carbohydrate fraction of soy

* Corresponding author at: Universidad Nacional de Rosario, Área Química General, Departamento de Químico-Física, Facultad de Ciencias Bioquímicas y Farmacéuticas, Suipacha 531, S2002LRK Rosario, Santa Fe, Argentina.
Fax: +54 341 4350214.
E-mail addresses: bellu@iquir-conicet.gov.ar, sbellu@fbioyf.unr.edu.ar (S.E. Bellú).

http://dx.doi.org/10.1016/j.jece.2015.12.008
2213-3437/

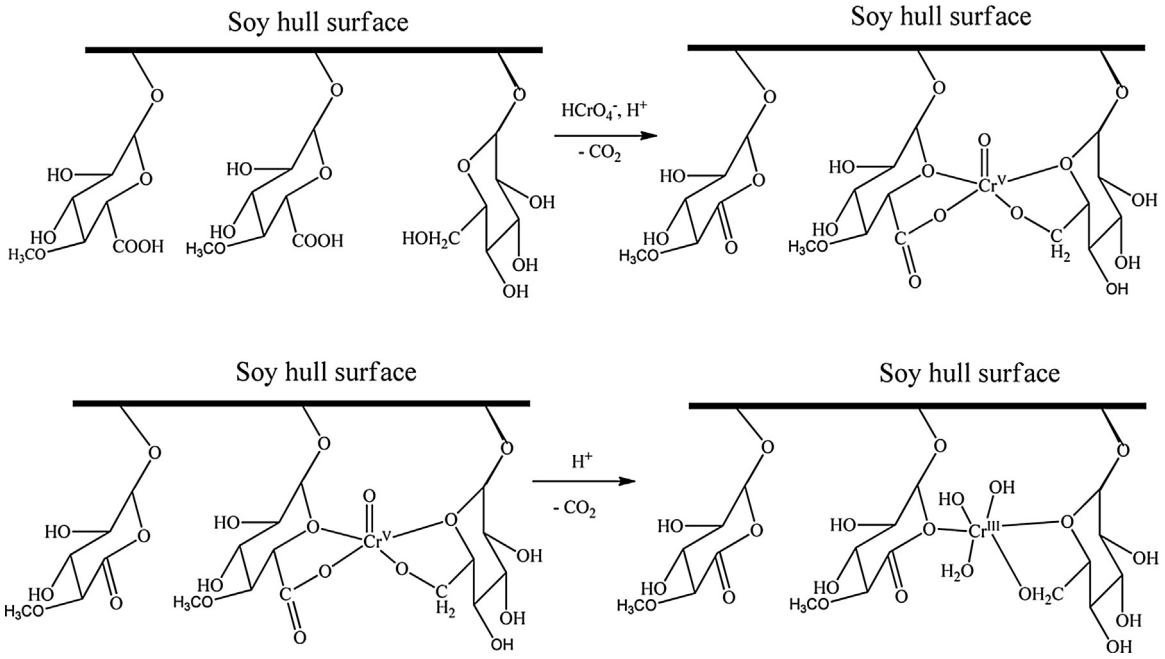

Scheme 1. Proposed mechanism for Cr^{VI} removal by soy hull biomass.

hull consists of 30% pectin, 50% hemicellulose, and 20% cellulose [19]. This fact makes soy hull a suitable biomass for metal biosorption. Soy hulls are an agro-industrial by-product available in great quantities in many countries, which could be used in waste-waters treatment processes. Additionally, it is a very cheap material lowering the costs involved.

The aim of the present work was to evaluate Cr(VI) removal from aqueous solution in batch and continuous systems using soy hull biomass. This biomass was chosen because it is obtained in great quantities, it is a cheap material and it contains a large number of biopolymers in its surface capable of binding and reducing Cr(VI) species. These characteristics make this biomass suitable for being employed in remediation of Cr(VI) contaminated waters. In this work we evaluated optimal conditions for batch removal of Cr(VI), kinetic and isotherm profiles, gathered spectroscopic evidence of a redox removal mechanism and analyzed the application of fixed bed columns in continuous Cr (VI) sorption removal.

2. Materials and methods

$K_2Cr_2O_7$ (Mallinckrodt, p.a.), $HClO_4$ ($\delta = 1.67\ g\ mL^{-1}$, 70% P/P) (Merck), NaOH (Cicarelli, p.a.), H_2SO_4 ($\delta = 1.84\ g\ cm^{-3}$, 98% P/P) (Merck), ethanol (Cicarelli, p.a.), K_2CO_3 (Sigma, p.a.), Na_2CO_3 (Sigma, p.a.), $AgNO_3$ (Cicarelli, p.a.), $K_2S_2O_8$ (Mallinckrodt, p.a.), H_2O_2(ac) 100 vol. (Cicarelli, p.a.), 1,5-diphenylcarbazide (Sigma, p. a.), diphenylpicryllhydrazyl (dpph) (Sigma, 99.9%), ehba = 2-ethyl-hydroxybutanoic acid (Aldrich 99.0%), $Cr(NO_3)_3{\cdot}9H_2O$ (Sigma, p.a.), were used without further purification. $Na[Cr^{(V)}O(ehba)_2]{\cdot}H_2O$(s) was synthesized as described in literature [20].

Aqueous solutions were prepared in milli Q deionized water. For experiments performed in the 1.00–4.00 pH range, the pH of the solutions was adjusted by addition of $HClO_4$. The concentration of stock solutions of perchloric acid was determined by titration employing standard analytical methods.

Caution: $K_2Cr_2O_7$, $Na[Cr^{V}O(ehba)_2]{\cdot}H_2O$, and dpph are human carcinogens. Contact with skin and inhalation must be avoided.

2.1. Preparation of the biomass

Soy hulls were collected from a neighboring harvest zone of Rosario, Santa Fe Province, Argentina. The biomass was submitted to mechanical milling in order to obtain 0.3–0.5 mm-sized pieces, washed with deionized–distilled water several times and then air-dried for several days. To determine the pH value at point of zero charge (pHzpc), 2.0 g of biomass was put into contact with 100 mL 0.10 M $NaNO_3$ solution with different pH values (2.0–9.0) at $T = 25\ ^\circ C$. The suspensions were stirred for 48 h (250 rpm). The change of pH (ΔpH) was calculated as a difference between the initial pH and the equilibrium pH values. The pHzpc was identified as the initial pH with minimum ΔpH [21].

2.2. Experimental design strategy. Response surface design

The response surface approach is desirable to find a mathematical model capable of predicting the response. The optimized model was obtained by using the Central Composite Design (CCD) [22]. To do this, one should measure the response at some points of the working domain. The selection of these experimental points

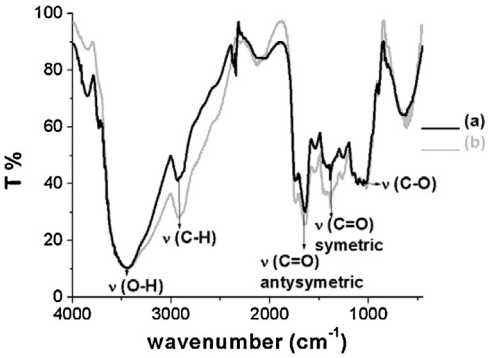

Fig. 1. FTIR spectra of (a) native soy hull, (b) Cr loaded soy hull.

needs prior knowledge and should be done carefully to map the experimental domain correctly. Through running CCD, a regression model was fitted to the response (mg Cr(VI) sorbed/g biomass). Such tests as lack of fit, analysis of variances (ANOVA), analysis of residuals distribution, over-fitting test, and coefficient of determination (R^2) were used to check the adequacy of the model [23,24]. All of the statistical and mathematical calculations were done by using Design Expert V. 7.0 software. Optimal conditions for sorption can be obtained by a visual or mathematical technique and when a suitable model has been found, the optimal conditions cab be visually or mathematically obtained. Also, a comparison between theoretical and experimental responses can be made.

2.3. Metal sorption experiments

Sorbent was suspended in 6.26 mg L^{-1} Cr(VI) solutions. The soy hull dose in the solution was of 20.0 ± 0.2 g L^{-1} (optimum dose obtained in CCD experiments). The soy hull/metal suspension was gently agitated (75 rpm) at controlled temperature, because at this speed maximum removal efficiency was obtained. The pH of the solution was adjusted to the desired value by adding $HClO_4$ 1.0 M. After a determined time, samples were taken from the solutions, and the Cr(VI) concentration in the supernatants was determined spectrophotometrically at 540 nm by using a double-beam UV–vis spectrophotometer (JASCO V-550 model) after complexation with 1,5-diphenylcarbazide in acid medium [25]. To measure total chromium concentration, the Cr(III) was firstly converted to Cr(VI) at high temperature (80 °C) by the addition of 1.00 mL H_2SO_4 (ac) 1.0 N, 50 μL $AgNO_3$ 2.0% P/V and 0.3 g $K_2S_2O_8$. The excess of $K_2S_2O_8$ was eliminated by boiling the reaction mixture at 100 °C, prior to the 1,5-diphenylcarbazide reaction. The Cr(III) concentration was the calculated from the difference between the total Cr content and Cr(VI) concentration, at different times.

Kinetic studies were carried out in a glass beaker with magnetic stirring at three temperatures (10, 25 and 40 °C). 2.0 g of biomass was added to 100 mL of Cr(VI) solution and keeping the suspension at constant pH throughout the experiment. The assays were carried out at three different pH values (1.00, 2.00 and 3.00). Samples (100 μL) of supernatant were taken at suitable time intervals and then analyzed for Cr(VI) concentration.

Isotherm assays were carried out at three different temperature values (20, 40 and 60 °C), varying the initial concentration of metal from 0.10 to 1000 mg L^{-1} (sorbent dosage = 20.0 g L^{-1}, pH 1.5). Upon reaching equilibrium, a sample (1 mL) was taken from supernatant and then analyzed for Cr_{total} concentration.

Metal uptake (q_e, mg g^{-1}) was calculated using the general definition, Eq. (1):

$$q_e = \frac{(C_0 - C_e)V}{m} \quad (1)$$

where C_0 and C_e are the Cr_{total} concentrations in solution (mg L^{-1}) at initial and equilibrium time, respectively, V is the solution volume (L), and m is the mass of the sorbent used (g).

2.4. Column experiments

The sorption of Cr(VI), by soy hull packed in glass columns of 15 cm long and 2.3 cm of internal diameter was studied. At the bottom end of the column a fiberglass cap was placed to avoid biomass particles losses. The columns were filled, and later compacted by gravity with soy hull, keeping constant the package density. The bottom of the column was connected to a peristaltic

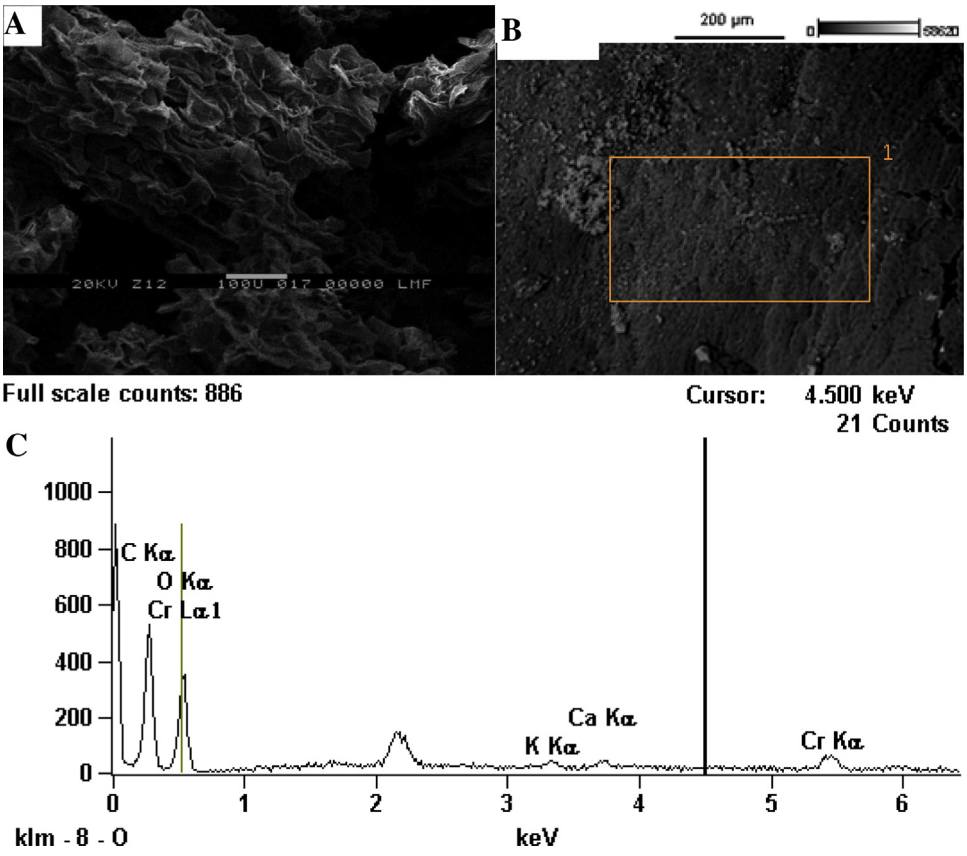

Fig. 2. Soy hull SEM images. (A) Before Cr(VI) sorption; (B) after Cr(VI) sorption. HV 20.0 KV and magnification 298×. C: EDAX analysis for Cr(VI) loaded soy hull.

pump (Gilson) using a silicone tube to obtain a constant steady upward flow of 2.5 mL min^{-1}. Solutions of a known concentration of Cr(VI) were pumped through the columns at constant pH 1.5 and room temperature. Samples of 1.0 mL were collected at time intervals to assess the residual concentration of metals and to determine the retained amount of metal. The sorption capacity of Cr(VI) was determined from Eq. (2).

$$q = \frac{C_{in}Q}{1000\,m}\int_0^t (1 - \frac{C_{out}}{C_{in}})dt \quad (2)$$

where q is the mass of metal sorbed (mg Cr(VI) g biomass^{-1}); C_{in} is the inlet solution concentration (mg L^{-1}); C_{out} the outlet solution concentration (mg L^{-1}); m is the amount of biomass in the column (g) and Q is the volumetric flow (mL min^{-1}).

In most industrial wastewater treatment units, a continuous mode of operation is preferred. The column bed performance is usually described through the concept of a breakthrough curve, which is obtained by plotting C/C_0 against time (C and C_0 are concentration of the outlet and inlet solutions at the column, respectively). Breakthrough and saturation time, sorption yield (%), and Cr(VI) ions uptake are relevant parameters that can be obtained from the breakthrough curve as follows:

Breakthrough time (t_b, min) is considered when outlet Cr(VI) concentration reaches the allowable limit (0.1 mg L^{-1}). Saturation time (t_{sat}, min) is usually considered when the effluent concentration remains close to influent concentration for a long period (corresponding to $C/C_0 = 0.95$). The uptake capacity (q_{ads}, mg g^{-1}) is obtained by dividing the quantity of Cr(VI) sorbed (m_{ads}) by the sorbent mass (m) (Eq. (3)).

$$q_{ads} = \frac{m_{ads}}{m} \quad (3)$$

where the total quantity of Cr(VI) sorbed by the biomass in the column (m_{ads}, mg) is calculated by subtraction of the quantity of Cr (VI) joined at the column (m_{inlet}, mg) and the quantity of Cr(VI) going out the column (m_{outlet}, mg) (Eq. (4)–(6)).

$$m_{inlet} = C_0 Q t_{sat} \quad (4)$$

$$m_{outlet} = Q\int_0^{tsat} (C_0 - C)dt \quad (5)$$

$$m_{ads} = m_{inlet} - m_{outlet} \quad (6)$$

Various simple mathematical models have been developed to describe and possibly predict the dynamic behavior of the column bed. Thomas model is one of the most general and widely used models in column performance theory. The model assumes Langmuir model of sorption–desorption, that no axial dispersion occurs and that the rate driving force obeys pseudo-second order reversible reaction kinetics [26].

The expression of Thomas model is given in Eq. (7).

$$\frac{C_t}{C_0} = \frac{1}{1 + \exp\left(\frac{(q_{Th}m - C_0 vt)k_{Th}}{v}\right)} \quad (7)$$

where k_{Th} (mL min^{-1} mg^{-1}) is Thomas rate constant, q_{Th} (mg g^{-1}) is the theoretical saturated sorption capacity in Thomas model, v (mL min^{-1}) is the flow rate of the effluent, m (g) is the mass of the sorbent, C_0 (mg L^{-1}) is the influent Cr(VI) concentration, C_t (mg L^{-1}) is the effluent Cr(VI) concentration at time t (min). The value of C_t/C_0 is the ratio of effluent and influent Cr(VI) concentrations at certain time. The kinetic coefficient k_{Th} and the sorption capacity of the column q_{Th} can be determined from a plot of C_t/C_0 against t at a given flow rate using non-linear regression.

Modified dose–response model minimized the error that results from use of the Thomas model, especially with lower and higher breakthrough curve times [27]. Its equation can be described as shown in Eq. (8).

$$\frac{C_t}{C_0} = 1 - \frac{1}{1 + (\frac{vt}{b})^a} \quad (8)$$

where v (mL min^{-1}) is the flow rate of the effluent. Parameters a and b comes from the modified dose–response model.

In order to provide information about the stability of the sorbent, DOC (dissolved organic carbon) concentrations in the leachates were measured in column effluents. DOC concentrations were analyzed in a TOC-V_{WS} (SHIMADZU). Effluent samples were filtered through a 0.2 mm membrane prior to the analysis. DOC concentrations in the leachates were less than 0.01 mg mL^{-1}, indicating that sorbent packed in the column is very stable.

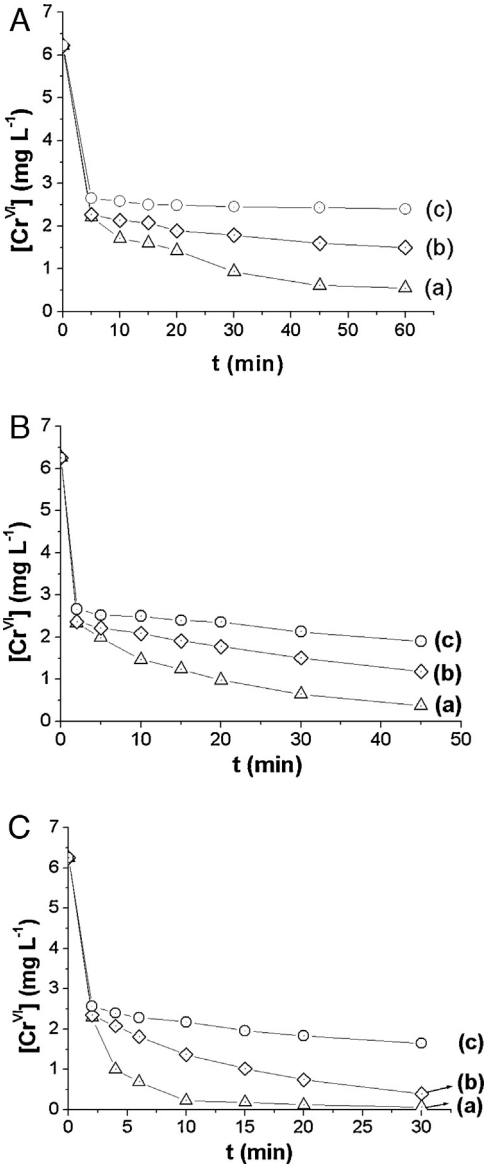

Fig. 3. Effects of pH on the Cr(VI) removal in aqueous phase at three temperature values. $[Cr(VI)]_0 = 6.30$ mg L^{-1}, $[Biomass]_0 = 20.00$ g L^{-1}. Fig. 2A: $T = 10$ °C, (a) pH = 1.0, (b) pH = 2.0 and (c) pH = 3.0. Fig. 2B: $T = 25$ °C, (a) pH = 1.0, (b) pH = 2.0 and (c) pH = 3.0. Fig. 2C: $T = 40$ °C, (a) pH = 1.0, (b) pH = 2.0 and (c) pH = 3.0.

2.5. Spectroscopic characterization

X-ray photoelectron spectroscopy (XPS) of a given sample was made with a spectrometer SPECS system equipped with a hemispherical energy analyzer, a nine channeltron detector System and a double anode X-ray source. A consistent 3.0 mm sized spot was analyzed on all surfaces; using an Mg Kα line at 1253.6 eV. The base pressure of 5.10^{-9} mbar raised up to 1.0×10^{-8} mbar when the samples were introduced in the chamber and irradiated with a power of 100 W. The calibration of the binding energy of the spectra was performed with the C1s peak of the aliphatic carbons: 284.6 eV. The sample was vacuum desiccated at 323 K for 24 h and then ground into powder for further XPS analysis. $Cr(NO_3)_3{\cdot}H_2O(s)$, $Na[Cr^{(V)}O(ehba)_2]{\cdot}H_2O(s)$ and $K_2Cr_2O_7(s)$ were used as Cr(III), Cr(V) and Cr(VI) references compounds, respectively.

X-ray Absorption Spectroscopic (XAS) experiments at the Cr K-edge (5898 eV) were carried out at beamline BL-9A with ring energy of 2.5 GeV and a ring current of 450 mA. A double-crystal Si (1 1 1) monochromator was used, and the beam was focused using a pair of bent conical mirrors coated with Rh [28]. The XAS spectra of Cr-laden soy hull were recorded in transmission mode, with N_2-He (30: 70) gas for the I_0 chamber and N_2 gas for the 1 chamber to monitor the incident and transmitted X-rays, respectively. The X-ray absorption near edge structure (XANES) spectra were measured with 0.35 eV steps and 1.0 s collecting time between 5980 and 6060 eV, while Extended X-Ray Absorption Fine Structure (EXAFS) spectra were measured with 2.5 eV steps and 4.0 s in transmission mode collecting time between 5500 and 7080 eV. EXAFS data-were analyzed with commercially available software (REX2000 program, Rigaku Co). The reference samples, the same employed for XPS measurements, were used to compare their spectral shapes and to identify major Cr species on the biomass surface [29].

Electronic paramagnetic resonance (EPR) spectra of soy hulls treated with Cr(VI) at different contact times were obtained with a Bruker ESP 300 E computer-controlled spectrometer operating at X-band frequencies (~9.4–9.8 GHz). Microwave generation was by means of a klystron (ER041MR) and frequencies were measured with a built-in frequency-counter. Spectra were recorded as first derivatives of the microwave absorption in 1024 points at 288 K, using 10 mW microwave power and 100 kHz modulation frequency. Power values used in the EPR experiments did not overcome 10 mW in order to avoid signal saturation. In EPR measurements, scanning speed and number were fixed in order to reduce the time each measure took. This was done to avoid fluctuations in the EPR signal during the sample scanning. *g*-values were determined by reference to dpph (g_{iso} = 2.0036) as an external standard. The modulation amplitude used for detection of paramagnetic oxo-Cr(V)-soy hull species was 2.0 G in order to increase the signal/noise ratio.

The surface structure of sorbent: soy hulls, before and after sorption of chromium was analyzed by scanning electron microscopy (SEM) coupled with energy dispersive X-ray (EDAX) analysis. Leitz AMR 1000 equipped with silica/lithium dispersive detector of X-ray at 200× magnification coupling to analyze and computer EDAX. The metal-loaded biomass samples were mounted on a stainless steel stab with double stick tape with a thin layer of gold in high vacuum conditions.

A qualitative analysis of the main functional groups that might be involved in metal binding could be assessed by Fourier transformed infrared (FT-IR) analysis. The soy hull biomass spectra, before and after sorption of Cr^{VI} were recorded with a Perkin Elmer FT-Spectrum One spectrometer. 5.0 mg of dried biomass was mixed and ground with 150 mg of KBr in an agate mortar. The tablets were analyzed in the 3600 and 400 cm^{-1} region, with 10 scans and spectral resolution of 4 cm^{-1} in the transmittance mode.

3. Results and discussion

3.1. FTIR analysis

The FT-IR spectra of free and Cr-loaded biomass after treatment of soy hull with Cr(VI), were measured in order to obtain information on the nature of possible interactions between the functional groups of soy hull and the metal ion, Fig. 1.

The FTIR spectrum of soy hull exhibits a broad peak at 3444 cm^{-1}, which corresponds to the O–H stretching vibrations of cellulose, pectin, absorbed water, hemicellulose, and lignin. The OH stretching vibrations appears at a broad range of frequencies, corresponding to free and bonded hydroxyl groups of carboxylic acids [30,31]. The band at 2929 cm^{-1} indicates symmetric or asymmetric CH stretching vibration of aliphatic compounds. Bands around 1740 and 1647 cm^{-1} are indicative of the presence of free and esterified carboxyl groups [32], respectively. The peak at 1407 cm^{-1} may be assigned to symmetric stretching of —COO^-. The band observed at 1054 cm^{-1} was assigned to C—O stretching of alcohols [33]. When the biomass was loaded with Cr, the FT IR spectrum showed some changes. The peak at 3444 cm^{-1} assigned to O—H stretching was broadened and the position of C—O vibrations was shifted 33 cm^{-1} to lower frequencies suggesting that hydroxyl groups are involved in the coordination of chromium at the surface of soy hulls. In the Cr-treated soy hulls spectra the intensity of the two bands at 1644 and 1410 cm^{-1}, corresponding to the asymmetric and symmetric stretching modes of carboxylate, strengthened relative to those of free carboxylic groups, suggesting that Cr is also sorbed on carboxylate sites of the biomass surface.

3.2. Surface characterization

The SEM images for the soy hulls before metal sorption showed a regular surface with robust consistency, Fig. 2.

However, after Cr(VI) treatment, Cr-laden soy hulls exhibited a changed surface morphology with evident rough structures. In comparison with the untreated soy hulls, the surface was flattened and micro-structures of the edges disappeared. These results are in agreement with those reported by Murphy et al. [34], who observed changes in surface morphology of seaweeds after treatment with Cr(III) and Cr(VI). Changes in surface morphology were due to binding of Cr(VI) ions to surface biopolymers, causing relaxation of the soy hull structure, thus leading to flattening of the surface. Soy hull contains cellulose in their cell wall with an extracellular matrix consisting of various polysaccharides, predominately pectin [19]. All these changes in the surface morphology indicated that some rearrangement of surface polymers occurs.

The presence of Cr on the surface of soy hull was confirmed by EDAX analysis. Semiquantitative analysis of Cr content gives 1.57% which is in agreement with the experimental Cr content value (1.65%).

Table 1
Rate coefficients of the removal reaction of Cr(VI) by the biomass at various pH and temperature values.

		10 °C	25 °C	40 °C
pH 1.0	k (L mol^{-1} min^{-1})	1.30 ± 0.04	1.98 ± 0.05	7.89 ± 0.03
	R^2	0.9915	0.9980	0.9959
pH 2.0	k (L mol^{-1} min^{-1})	0.40 ± 0.02	0.72 ± 0.07	2.77 ± 0.02
	R^2	0.9910	0.9997	0.9998
pH 3.0	k (L mol^{-1} min^{-1})	0.10 ± 0.01	0.35 ± 0.01	0.76 ± 0.02
	R^2	0.9905	0.9901	0.9957

3.3. Improvement of Cr(VI) removal with central composite design

In order to improve Cr(VI) removal, the central composite design was applied to select experiments (see Table S1, Supplementary material).

Data were analyzed using multiple regression analysis. The relationship between Cr(VI) removal (q) and the test variables was:

$$q = 0.734 - 0.0754\text{pH} + 0.0149\text{m} + 2.54 \times 10^{-3}\text{t} - 0.0434\text{pH}^2 - 0.0217\text{m}^2 + 0.0446\text{pH m} - 5.11 \times 10^{-4}\text{m t} \quad (9)$$

To validate the regression coefficient, analysis of variance was performed. The model F-value of 87.2 implies that the model is significant. Values of Prob > F less than 0.0500 suggest that the model terms are significant (see Table S2, Supplementary material). R^2 of the model was 0.9823, which is considered as very good correlation. Therefore, it is justifiable to apply the model to predict the responses.

The 3D surface plot was obtained applying Eq. (9), from which the Cr(VI) removal, at different contact time, sorbent doses and pH values can be predicted (see Fig. S1, Supplementary material). Good correlation between calculated and observed values was obtained (see Fig. S2, Supplementary material)

The results showed that the maximum value of Cr(VI) removal was obtained at pH 1.5, sorbent dose = 20.0 g L^{-1} and contact time = 120 min. At pH 1.5, the major Cr(VI) specie is $HCrO_4^-$ (see Fig. S3 Supplementary material) as calculated by HYDRA and MEDUSA Programs [35]. The point of zero charge (pHzpc) is the solution pH value, where the surface charge density is equal to zero. If pH < pHzpc the sorbent surface area is positively charged, and if pH > pHzpc, the sorbent surface area is negatively charged [36]. The point of zero charge (pHzpc) is the value at which the curve ΔpH = f (pHi) intersects pHi axis (see Fig. S4, Supplementary material).

The obtained pHzpc value was 5.7. As consequence, at pH value less than 5.7, the surface area of soy hull is positively charged and, at pH values employed in the present work strongly attracts the negatively charged $HCrO_4^-$ specie.

In order to verify the improved effect by statistically designed experiments, a reaction with recipes at optimal conditions was performed. The experimental q value obtained (0.80 mg Cr(VI)/g biomass) was in agreement with the calculated value using Eq. (9) ($q = 0.734 - 0.0754 \times 1.5 + 0.0149 \times 2 + 2.54 \times 10^{-3} \times 120 - 0.0434 \times (1.5)^2 - 0.0217 \times (2)^2 + 0.0446 \times 1.5 \times 2 - 5.11 \times 10^{-4} \times 2 \times 120 =$ 0.78 mg Cr(VI)/g biomass). This similarity between the predicted and observed result reflects the accuracy and applicability of the central composite design as an extremely powerful method for optimizing the Cr(VI) sorption onto soy hull surface.

3.4. Reduction of Cr(VI) to Cr(III) by soy hull biomass. Influence of pH and T

Cr(VI) is a strong oxidant and in presence of organic matter it reduces to Cr(III). Many authors had studied removal of Cr(VI) employing different biomasses and in all cases they report reduction of Cr(VI) to Cr(III) [37–39]. To obtain kinetic parameters of the redox reaction between Cr(VI) and soy hull surface, the Cr (VI) concentrations profiles were performed at three different pH and temperature values (Fig. 3).

The Cr(VI) concentration was found to sharply decrease, and this reaction was acid catalyzed.

At a fixed pH value, the redox reaction rate was higher at high temperature values. In general, the increase of temperature increases the rate of a redox reaction [40].

In order to measure the Cr(VI) -reducing capacity of soy hull, 0.500 g of biomass was put into contact with 100 mL Cr(VI) solution (302.8 mg L^{-1}) at pH = 1.0 and T = 25 °C (see Table S3, Supplementary material).

Working with an excess of Cr(VI) oxidant, we were able to determine Cr(VI) -reducing capacity, and the obtained value 58.4 ± 0.5 mg of Cr(VI)/g soy hull, at 25 °C.

3.5. Kinetic model

A kinetic model for the Cr(VI) removal by different biomasses was developed by Park et al. [38,41]. This model considers first order in [Cr(VI)] and first order in [biomass]. Eq. (10) gives the integrated form of this kinetic model:

$$\frac{\ln\left(\frac{[\text{Cr(VI)}]_0(C^*_{OC}[B]-[\text{Cr(VI)}]_0+[\text{Cr(VI)}])}{C^*_{OC}[B][\text{Cr(VI)}]}\right)}{C^*_{OC}[B]-[\text{Cr(VI)}]_0} = kt \quad (10)$$

where $[Cr(VI)]_0$ is the initial concentration of Cr(VI), [Cr(VI)] is the concentration of Cr(VI) at time = t, [B] is the biomass concentration, C^*_{OC} is the content of equivalent organic compound per unit gram of biomass, i.e. C^*_{OC} of soy hull is 1.12 ± 0.01 mmol g^{-1} (see Table S3, Supplementary material), and k is the rate constant (L mol^{-1} min^{-1}).

The values for the dependent variable were calculated and plotted against time, t (see Fig. S5, Supplementary material), for different batch conditions.

These curves were nearly linear (R^2 higher than 0.99), indicating that the employed model was in agreement with experimental data.

For the conditions where pH and temperature were varied, the rate coefficients, k, were calculated and are shown on Table 1.

Park et al. [38], demonstrated that the reaction rate constant is strongly pH and T dependent (Eq. (11)), and that a linear correlation exists between the reaction rate logarithm with the pH and T^{-1} values, according to Eq. (12):

$$k = f(\text{H}^+, T) = A[\text{H}^+]^n e^{-\frac{E_a}{RT}} \quad (11)$$

$$\ln(k) = \ln(A) + n\ln([\text{H}^+]) - \frac{E_a}{RT} \quad (12)$$

where A, E_a, R, T and n are the frequency factor, activation energy (J mol^{-1}), gas constant (8.314 J mol^{-1} K^{-1}), Kelvin temperature (K) and order of reaction respect to [H^+], respectively.

Plot of ln(k) versus ln([H^+]) and 1/T yield a plane shape (See Fig. S6, Supplementary material).

Fitting experimental data with Eq. (12), we obtained constant values of $A = e^{(21\pm2)}$, $n = 0.48 \pm 0.04$ and $E_a = 47 \pm 5$ kJ mol^{-1}. The correlation coefficient value of 0.9868 confirmed an adequate representation of the data by the employed model.

Combining Eq. (10) and (11) it is possible to obtain a complete kinetic model that describes [Cr(VI)] vs time profiles (Eq. (13)).

$$[\text{Cr(VI)}] = \frac{C^*_{OC}[B][\text{Cr(VI)}]_0 - [\text{Cr(VI)}]_0^2}{C^*_{OC}[B]e^{\left(A[\text{H}^+]^n e^{-\frac{E_a}{RT}}\left(C^*_{OC}[B][\text{Cr(VI)}]_0 - [\text{Cr(VI)}]_0\right)t\right)} - [\text{Cr(VI)}]_0} \quad (13)$$

Eq. (13) and the obtained parameter values were used to model the [Cr(VI)] vs t profiles in aqueous phase, employing soy hulls as reductant (see Fig. S7, Supplementary material).

Table 2
Weber Morris kinetic model of Cr(VI) biosorption onto soy hull.

C_0 (mg L^{-1})	k_{d1ff} (mg g^{-1} $min^{-1/2}$)	R^2	C
10	0.02	0.84	0.21
20	0.05	0.77	0.47
50	0.02	0.70	1.89

Table 3
Characteristic parameters of the different isotherm models and coefficients of determination (R^2).

	T 20 °C	T 40 °C	T 60 °C
Langmuir			
q_m (mg g^{-1})	7.286 ± 0.005	21.2 ± 0.3	21.8 ± 0.1
K_L (L mg^{-1})	0.007 ± 0.001	0.008 ± 0.002	0.031 ± 0.006
R_L	0.152	0.172	0.0606
R^2	0.9822	0.9846	0.9847
Freundlich			
K_F	0.43 ± 0.08	1.2 ± 1	2.6 ± 0.6
$1/n$	0.41 ± 0.03	0.44 ± 0.02	0.36 ± 0.04
R^2	0.9848	0.9957	0.9591
D–R			
q_m (mg g^{-1})	12.4 ± 0.9	40 ± 2	41 ± 3
β(mol^2 J^{-2}) x 10^9	6.1 ± 0.5	5.4 ± 0.3	3.4 ± 0.3
E (kJ mol^{-1})	9.05 ± 0.02	9.6 ± 0.1	12.1 ± 0.3
R^2	0.9958	0.9934	0.9808
Redldich–Peterson			
K_{RP} (L g^{-1})	0.92		
a_{RP} (L mg^{-1})	3.2		
β_{RP}	0.91		
R^2	0.9809		
Sips			
q_{max} (mg g^{-1})	9.71		
K_s	0.003		
γ	0.82		
R^2	0.9675		

Biomass doses 20.0 g L^{-1}; pH = 1.5; contact time: 6 h; $[Cr(VI)]_0$ = 0.10–1000.00 mg L^{-1}.

As shown in this figure, the model gave a good fit to the experimental data. The same model applied in the present work was previously applied to the study of Cr(VI) removal by *Laminaria digitata* algae [39], pine needle [41], and *Corynebacterium glutamicum* biomass [42]. In all cases, the model employed showed a good representation of the experimental data, regardless of the types of biomasses.

Theoretical treatments of intraparticle diffusion yield rather complex mathematical relationships which differ in form as functions of the geometry of the biosorbent particle. A functional relationship common to most treatments of intraparticle diffusion is that uptake varies almost proportionately with the square root of time, $t^{0.5}$, rather than t; a nearly linear variation in the quantity biosorbed with $t^{0.5}$ is predicted for a large initial fraction of reactions controlled by rates of intraparticle diffusion. The most-widely applied intraparticle diffusion equation for biosorption system is given by Weber and Morris [43]:

$$q_t = k_i t^{1/2} + C \quad (14)$$

where k_i is the intraparticle diffusion rate constant (mg g^{-1} min$^{0.5}$) and the intercept C, obtained by extrapolation of the linear portion. Experimental data were fitted through this model, the correlation coefficients R^2 values ranged from 0.84 to 0.70, the straight lines

Table 4
Comparison between the sorption of Cr(VI) ions by soy hull and other sorbents reported in literature.

Sorbent	Cr(VI) uptake (mg/g)	Reference
sawdust	41.52	[15]
Nanoporous activated neem bark	26.95	[54]
Heat killed *Acinetobacter junii*	8.003	[55]
Tea waste	2.074	[56]
Date pits	1.853	[56]
Polyphenol-SiO_2	4.500	[57]
Iron oxide membrane	0.210	[58]
Fly ash coated by chitosan	2.670	[59]
Copper coated polymer foam	9.160	[60]
Magnetic alginate hybrid beads	9.166	[61]
Soy hull	7.286	This work

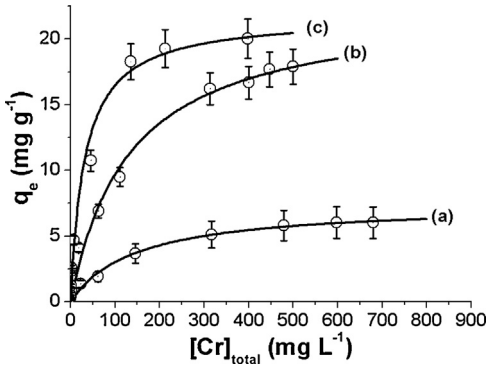

Fig. 4. Sorption isotherm of Cr(VI) onto soy hull. Biomass doses = 20.0 g L^{-1}; pH = 1.5; $[Cr(VI)]_0$ = 0.10–1000.00 mg L^{-1}; contact time 2 h. ———— Langmuir model; (a) 20 °C; (b) 40 °C; (c) 60 °C.

obtained when fitting experimental data did not pass through the origin, also indicating that pore diffusion was not the only rate-controlling step. (Table 2).

3.6. Sorption isotherms

Sorption isotherms represent the dynamic equilibrium of solution free and surface boundary sorbate on different biomass. Sorption isotherms are often used as empirical models, in this work Langmuir, Freundlich and Dubinin–Radushkevich (D–R) were using to describe the Cr(VI) uptake by soy hull biomass.

Langmuir isotherm is given by Eq. (15) [44]:

$$q_e = \frac{q_m K_L C_e}{1 + K_L C_e} \quad (15)$$

C_e represents the equilibrium concentration of Cr_{total} (mg L^{-1}), the quantity of necessary metal to produce a monolayer on the surface of the sorbent is q_e (mg g^{-1}), K_L is the Langmuir equilibrium constant (L mg^{-1}). The essential characteristics of Langmuir adsorption isotherm can be expressed by means of a dimensionless constant, equilibrium parameter or separation factor (R_L) which is defined by Eq. (16) [45], where, C_0 is the initial concentration of Cr (VI) (mg L^{-1}).

$$R_L = \frac{1}{1 + K_L C_0} \quad (16)$$

As the R_L values lie between 0 and 1, the sorption process is favorable.

Additionally, experimental adsorption data was fitted to Freundlich isotherm model.

The exponential form of Freundlich adsorption isotherm is given below, Eq. (17) [46].

$$q_e = K_F C_e^{1/n} \quad (17)$$

where C_e is the equilibrium concentration of metal ions (mg L^{-1}), q_e is the amount of metal ions required for forming a monolayer onto the sorbent surface (mg g^{-1}), K_F and $1/n$ are Freundlich equilibrium constants related to the adsorption capacity and adsorption intensity.

The Dubinin–Radushkevich (D–R) model is used extensively to describe sorption processes. The D–R is shown in Eq. (18) [47].

$$q_e = q_m e^{-\beta\varepsilon^2} \quad (18)$$

The constant, β (mol^2 J^{-2}), is related to the mean free energy of sorption per mole of the sorbate and q_m represent the theoretical saturation capacity. This equation also includes the Polanyi potential, ε, which correspond to [RT ln(1 + 1/C_e)], being R (J mol^{-1} K^{-1}) the gas constant and T (K) the absolute temperature.

The free energy of sorption, E (kJ mol^{-1}), can be calculated using Eq. (19) [48]. This approach was usually applied to distinguish the physical and chemical adsorption process.

$$E = \frac{1}{(2\beta)^{1/2}} \quad (19)$$

When the value of E, is in the range 8–16 kJ mol^{-1}, the sorption process is a chemical ion-exchange process, while for E values <8 kJ mol^{-1}, the sorption mechanism occurs through a physical process. The E values at three different temperatures and the various constants of the three models were calculated and represented in Table 3.

Comparing the correlation coefficients, it can be concluded that D–R isotherm model provide the best model for the present sorption system. The maximum sorption capacity increases as T increases. This result was previously found for others systems [49,50], and it is attributed to an increase of available sorption sites. The value of the dimensionless parameter ($0 < R_L < 1$), indicates that sorption is favorable. The E values lies between 8 and 16 kJ mol^{-1}, as can be seen in Table 3, which suggests ion-exchange sorption mechanism [51].

In some cases, the available two parameters models are not adequate to correlate the equilibria data; therefore models with more than two parameters are required. The following three parameter isotherm models were used to describe the biosorption experimental data.

Redlich–Peterson isotherm model incorporated the features of the Langmuir and Freundlich isotherms into a single equation [52]. There are two limiting behaviors: Langmuir form for $\beta = 1$ and Freundlich form for $\beta = 0$.

$$q_e = \frac{K_{RP} C_e}{1 + a_{RP} C_e^{\beta}} \quad (20)$$

It is worth noting that the β value obtained in the present work was 0.91, i.e., the data can preferably be fitted with the Langmuir model. This is confirmed by the satisfactory fit of the data to the Langmuir model.

At low sorbate concentrations, Sips isotherm model effectively becomes the Freundlich isotherm. At high sorbate concentrations, it predicts a monolayer sorption capacity characteristic of the Langmuir isotherm [53].

$$q_e = q_{max} \frac{(K_S C_e)^{\gamma}}{(1 + (K_S C_e)^{\gamma})} \quad (21)$$

The exponent γ value was found to be 0.82; this means that the Cr(VI) sorption data obtained in this study is more of the Langmuir form rather than that of Freundlich, which was also confirmed by the results shown in Table 3.

Comparison of sorption capacity of soy hull biomass and various other sorbents is shown in Table 4.

Soy hull has a high sorption capacity, comparable with that of other sorbents. Therefore, considering the low cost of this natural sorbent (agriculture waste), it can be used as an alternative material to minimize the concentration of Cr(VI) concentration in groundwater and wastewater.

The isotherm profiles of Cr(VI) sorption at various T values are shown in Fig. 4.

3.7. Sorption thermodynamics

In engineering practice, values of thermodynamic parameters such as enthalpy change (ΔH°), entropy change (ΔS°) and free energy change (ΔG°) must be taken into consideration in order to determine the spontaneity of a process.

The sorption free energy change, ΔG° can be calculated using Eq. (22).

$$\Delta G^\circ = -RT \ln K_L \quad (22)$$

where K_L (L mol^{-1}) is the Langmuir constant, R (8.314 J mol^{-1} K^{-1}) is the universal gas constant, and T (K) is the temperature.

It is recognized that ΔG° is given as J mol^{-1}, and so the equilibrium constant K_L in Eq. (22) has to be dimensionless [62,63]. The K_L constant is simply recalculated as dimensionless by multiplying it by 55.5 (mol H_2O L^{-1}).

Taking into account the last consideration, ΔG° value is expressed as shown in Eq. (23).

$$\Delta G^\circ = -RT \ln(55.5 K_L) \quad (23)$$

The heat of sorption of the sorbent, ΔH° (kJ mol^{-1}), and entropy ΔS° (J mol^{-1} K^{-1}) for the sorption process is given in Eq. (24):

$$\Delta G^\circ = \Delta H^\circ - T\Delta S^\circ \quad (24)$$

For the determination of ΔH° and ΔS° the equation above can be written as shown in Eq. (25).

$$\ln 55.5 K_L = \frac{\Delta S^\circ}{R} - \frac{\Delta H^\circ 1}{R \ T} \quad (25)$$

The experimentally obtained thermodynamic data were ΔH° = +33.24 kJ mol^{-1} and ΔS° = +194.7 J K^{-1} mol^{-1} (see Table S4, Supplementary material).

The positive values of ΔS° and ΔH° calculated with Eq. (25), indicates an increase in disorder and the endothermic nature of the sorption processes, respectively. As a result, increasing the solution temperature will enhance the binding potential at equilibrium [64,65]. The endothermic sorption processes imply that diffusion from bulk solution to sorbent boundary will possibly involve energy to overcome interaction between water molecules and chromate ions [66,67]. Positive ΔS° values also indicate that an ion replacement reaction is taking place. The negative ΔG° value, point out that sorption processes were spontaneous in the studied temperature range.

3.8. Isosteric heat of sorption

Isosteric heats of sorption are key thermodynamic parameters when designing separation processes [68]. The heats can be high and complex functions of sorbate charges (q) when the sorbent is energetically heterogeneous. Ignoring these characteristics in process design can lead to serious errors [69]. The sorption heat determined for a constant amount of retained sorbate is known as the isosteric heat of sorption and can be calculated using

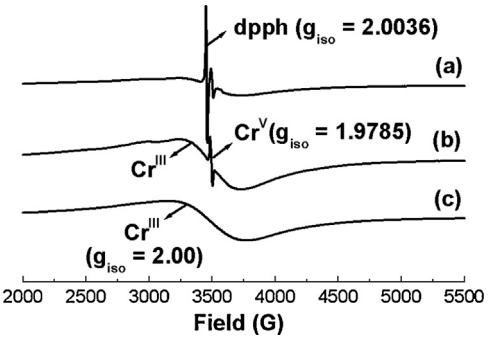

Fig. 5. EPR spectra of Cr-laden soy hull at different contact times. T = 15 °C; [biomass]$_0$ = 20.00 g L^{-1}, [Cr(VI)]$_0$ = 0.12 mM, pH = 2.0; center field = 3410 G; modulation amplitude = 2.0 G; resolution = 1024 points; frequency = 9.4312 GHz. Contact time: (a) 30 min, (b) 3 h and (c) 48 h.

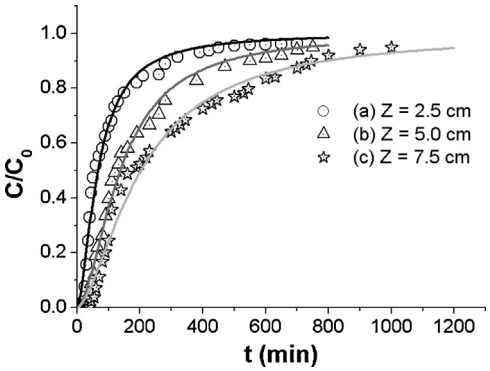

Fig. 6. Breakthrough curves and modified doses–response models for different bed heights. C_0 = 50 mg L^{-1} Cr(VI); Q = 2.50 mL min^{-1}; T = 20 °C; pH = 1.5. (a) h = 2.5 cm; (b) h = 5.0 cm; (c) h = 7.5 cm.

Clausius–Clapeyron equation [70] (Eq. (26)).

$$\frac{d\ln(C_e)}{dT} = -\frac{\Delta H_{st}}{RT^2} \quad (26)$$

Thus plots of ln C_e versus T^{-1} were derived for different amounts of adsorbed chromium and ΔH_{st} values were calculated from the slope of these isosters (See Fig. S8, Supplementary material).

Isosteric heat of sorption increases with q, indicating that soy hull biomass has an energetically homogeneous surface [71]. This increment occurs because at lower q values, sorbate–sorbent interaction takes place resulting in low ΔH_{st} values. As q increases, sorbate–sorbate interaction occurs resulting in an increment of heats of sorption [72,73].

3.8.1. Mechanism of Cr(VI) reduction by soy hull

Characterization of chromium oxidation state on the biomass surface would establish if Cr(VI) redox removal is the mechanism that governs the remediation process [74]. With that purpose in mind, XPS, XAS and EPR spectroscopy experiments were conducted.

High-resolution XPS spectra were collected from the Cr 2p core regions of the Cr-laden biomass as well as standard Cr(III), Cr(V), Cr (VI) (see Fig. S9, Supplementary material). $Cr(NO)_3$(s) (Cr(III) standard) gave spectra with bands appearing at binding energies 577 and 587 eV, the former corresponds to Cr $2p_{3/2}$ orbital, the latter to Cr $2p_{1/2}$ orbital. A signal that appears at binding energy 579 eV is characteristic of the XPS spectra of Cr(V) standard (Na[$Cr^{V}O(ehba)_2$]). Signals of standard Cr(VI) compound, $K_2Cr_2O_7$(s), appeared at binding energies of 579.5 and 590 eV. The Cr-loaded biomass spectra was coincident with the standard Cr(III) compound: $Cr(NO)_3$(s) (binding energies 576 and 586 eV), and there was no coincidence of Cr-loaded biomass with the standard Cr(V) compound. These results suggest that the chromium specie bound on the biomass was Cr(III).

Cr(V) is usually an unstable intermediate in the Cr(VI)/Cr(III) redox reaction, conducted by organic reducing agents. EPR spectra of Cr-loaded soy hull biomass at different contact times (see Fig. 5) showed the presence of an oxo-Cr(V)-biomass intermediate at short contact time (3 h).

Table 5
Different parameters for Thomas and Modified dose–response models.

Z (cm)	Thomas model			Modified dose–response model		
	k_{Th} x 10^4	q_{Th}	R^2	a	b	R^2
2.5	5.6 ± 0.3	2.1 ± 0.3	0.9227	1.65 ± 0.08	165.6 ± 0.3	0.9850
5.0	3.2 ± 0.4	1.25 ± 0.08	0.9255	1.67 ± 0.07	342.5 ± 0.4	0.9902
7.5	1.7 ± 0.3	0.73 ± 0.05	0.9101	1.69 ± 0.06	510.2 ± 0.3	0.9882

C_0 = 50 mg L^{-1} Cr(VI); Q = 2.50 mL min^{-1}; T = 20 °C; pH = 1.5.

Table 6
Different parameters for BDST model.

C_t/C_0%	k_{BDST} x 10^2 (L mg^{-1} min^{-1})	N_0 (mg L^{-1})	R^2
5	4.5 ± 0.4	252.0 ± 0.5	0.9992
20	3.4 ± 0.5	372.0 ± 0.4	0.9986
50	–	744.0 ± 0.8	0.9980
80	0.83 ± 0.06	2190 ± 1	0.9999

C_0 = 50 mg L^{-1} Cr(VI); v = 0.60 cm min^{-1}; T = 20 °C; pH = 1.5; z = 2.5; 5.0 and 7.5 cm.

The EPR spectral parameter, g_{iso}, depends on the Cr(V) coordination sphere [75]. EPR spectra exhibited a signal with g_{iso} = 1.9785, indicating that oxo-Cr(V) was coordinated to alcoholate and carboxylate groups, which may belong to the same or different polymeric chain presents in the biomass surface. At long contact time (48 h) only a typical broad signal corresponding to Cr (III) was detected (g_{iso} = 2.00), confirming the total reduction of Cr (VI) to Cr(III) onto the biomass surface.

X-ray Absorption Near-Edge Structure (XANES) is a technique used to determine principally oxidation state. The XANES spectra of Cr_2O_3 and $Cr(NO)_3{\cdot}9H_2O$ (s), were employed as references for the known oxidation state and chemical species of Cr(III). $K_2Cr_2O_7$ (s) and Na[$Cr^{V}O(ehba)_2$] were used as Cr^{VI} and Cr^{V} references respectively. Fig. S10 (Supplementary material) showed the normalized Cr K-edge XANES spectra of reference compounds and Cr-laden biomass.

The edge position of chromium compounds, determined by using the inflection point of the absorption threshold, is used to determine the energy positions of the resonances. The edge position increase from 5996.5 to 6000.2 and 6002.4 eV, in the following order Cr_2O_3, Na[$Cr^{V}O(ehba)_2$]·H_2O, $K_2Cr_2O_7$. XANES of spectra of Cr-loaded biomass have an edge position of 5996.8 eV. By comparison with the edge position of standard chromium compounds, a formal oxidation state of Cr(III) was assigned to the surface-bounded chromium. It can be seen that dichromate spectrum, Cr(VI), has a very intense pre-peak centered at 5987.3 eV. However, this pre peak was absent in Cr-loaded biomass. XANES spectra of Cr-loaded biomass have the same spectra features observed for $Cr(NO_3)_3{\cdot}9H_2O$(s) reference. This provides strong evidence that Cr(VI) adsorbed onto soy hull biomass was reduced to Cr(III), and this result is consistent with the XPS experiments.

EXAFS spectroscopy was used to determine the coordination sphere of Cr in Cr-loaded soy hull. The experimental Fourier transform results are shown in Fig. S11 (Supplementary material), and the curve-fitted parameters are given in Table S5 (Supplementary material).

For $Cr(NO)_3{\cdot}9H_2O$(s), the k^3 -weighted FT function gave a main peak centered at 1.60 Å which corresponds to first-shell oxygen back-scattering and another smaller peak centered at ~3.15 Å (phase-uncorrected). Three main peaks corresponding to oxygen shell (Cr—O) (1.60 Å), Cr type shell (Cr—Cr) (2.52 Å) and both Cr and O atoms (3.31 Å) were observed for the Cr_2O_3 compound. From Table S5 it is evident that the coordination number of chromium on the biomass was similar to that of Cr(III) compound, where Cr^{III} is hexa-coordinated. The Cr-O bond distances were almost the same lengths, which are in agreement to the Cr—O bond lengths reported in the literature [76–78].

In the present study, Cr(VI) was reduced to Cr(III), and completely removed from aqueous solution. XPS and XAS studies indicated that Cr bound on the biomass was Cr(III), implying that the removal of Cr(VI) occurs via redox reaction. Furthermore, EPR studies showed that Cr(VI) was reduced to Cr(V) bounded to the surface and, at long contact times, Cr(V) was completely reduced to

Cr(III). From the preceding experimental results, we proposed a mechanism of Cr(VI) removal by soy hull biomass showed in Scheme 1.

In the proposed mechanism, first $HCrO_4^-$ is attracted to the surface positively charged by ion-exchange, as suggested by D–R isotherm models. Once $HCrO_4^-$ species are on the surface, binding to —OH and —COOH occurs. Binding at hydroxyl and carboxylic functional groups were proposed based on IR evidence (frequencies assigned for these functional groups were modified after Cr (VI) uptake by soy hull) and on EPR evidence (g values corresponding to oxo-Cr(V) coordinated to hydroxyl and carboxylate groups). These functional groups are present in pectin and hemicelluloses polymers contained in the soy hull surface. Finally redox reaction occur, giving Cr(III) as final bounded species confirmed by EPR, XAS and XPS evidence.

3.9. Continuous sorption studies

The experimental breakthrough curves at three different bed heights and those obtained for the Modified dose–response model are represented in Fig. 6.

The experimental breakthrough time ($C/C_0 = 0.002$), saturation time ($C/C_0 = 0.95$), and Cr(VI) ions uptake ($mg\,g^{-1}$) obtained experimentally were tabulated in Table S6 (See Supplementary material). Thomas and modified dose–response parameters, and the correlation coefficients (R^2), are tabulated in Table 5.

It was found that the Thomas model (R^2) range from 0.910 to 0.926 exhibited an adequate fit of the experimental data. In order to improve the fit of the experimental data, modified dose response model was applied. As shown in Table 5, values of R^2 increase to 0.985–0.990 allowing an excellent fit of the experimental breakthrough curves. a and b values increased with an increase in bed height. Similar behavior was reported by Albadarin et. al [79].

The breakthrough time and the saturation time increase as bed height increases since a higher bed depth results in a longer residence time of the solution in the column.

3.10. Scale-up study

The bed depth service time (BDST) model predicts the relationship between the bed depth, Z (cm), and the operation time, t (min). This model assumes that the sorption rate is controlled by surface reaction between the sorbate and the unused capacity of the sorbent [80].

Eq. (27) expresses a linear relationship between the bed depth and the service time:

$$t = \frac{N_0}{C_0 v} Z - \frac{1}{k_{BDST} C_0} \ln\left(\frac{C_0}{C_t} - 1\right) \quad (27)$$

where N_0 is the sorption capacity ($mg\,L^{-1}$), v is the fluid velocity ($cm\,min^{-1}$) determined as the volumetric flow rate over the bed section area, C_t is the outlet concentration at time t ($mg\,L^{-1}$) and k_{BDST} is the kinetic constant ($L\,mg^{-1}\,min^{-1}$). k_{BDST} and N_0 can be calculated from the linear and angular coefficient, respectively, from the graph of t as a function of Z at a given C_t/C_0 ratio (iso-concentration line).

Iso-concentration lines for Cr(VI) ions removal in a fixed bed at $C_t/C_0 = 5$, 20, 50 and 80% were determined, (see Fig. S12, Supplementary material).

Table 6 showed the k_{BDST} and N_0 parameters obtained for different C_t/C_0 ratios.

A consistent increase in slopes from 8.4 to 73 was observed for C_t/C_0 ratios of 5–80% and a consequent increase in the corresponding dynamic sorption capacity N_0 from 252 to 2190 $mg\,L^{-1}$. On the sorbent used, some active sites remain unoccupied by Cr(VI) ions at lower C_t/C_0 ratio value, and hence the sorbent remained unsaturated. The dynamic sorption capacity in such low breakthrough condition was consequently bound to be lower than the full bed capacity of the sorbent [79]. The rate constant, k_{BDST}, characterized the rate of solute transfer from the fluid phase to the solid phase. Its value falls at higher C_t/C_0 ratio. This might be explained because during the initial phase Cr(VI) removal is fast and highly effective but decreases at higher C_t/C_0 ratio, as a consequence of the progressive saturation of the binding sites.

To further check the validity of BDST model the breakthrough curve was inspected at 50%. At 50% breakthrough, $C_o/C_t = 2$, therefore reducing the logarithmic term of BDST equation to zero. Good correlation coefficient was obtained at 50% breakthrough suggesting the conformity of BDST model with sorption of Cr(VI) by soy hull. Therefore, the constants obtained using the BDST model could be used to predict the times at which the ratio C_t/C_0 equals 0.05–0.80 for other bed depths.

The critical bed depth, Z_0 is calculated by setting $t = 0$ and $C_t = C_b$. It is given by Eq. (28).

$$Z_0 = \frac{v}{k_{BDST} N_0} \ln\left(\frac{C_0}{C_b} - 1\right) \quad (28)$$

The critical bed depth, Z_0 calculated from Eq. (28) was 0.2 cm. This value is the minimum theoretical bed height of the sorbent that is sufficient such that the effluent concentration at $t = 0$ will not exceed the breakthrough concentration, C_b.

4. Conclusions

In this work, principal aspects investigated included optimization of the sorption process, kinetics and sorption isotherms modeling, FTIR, SEM, XPS, EPR, XAS and EDAX analysis, continuous sorption and scale-up studies.

Optimization studies results in pH 1.5 and sorbent dose $20.0\,g\,L^{-1}$ as optimal conditions for Cr(VI) removal. FTIR analysis shows that hydroxyl and deprotonated carboxylic groups are involved in the coordination of chromium species at the surface of soy hull.

The equilibrium was described best by Langmuir model. The q_m value obtained was $7.286\,mg\,g^{-1}$ and it was comparable with that of the other sorbents reported in literature. Thermodynamic parameters reveal that the sorption process was spontaneous and endothermic. The isosteric heat of sorption increases with surface loading, indicating that soy hull has an energetically homogeneous surface.

High-resolution XPS spectra showed that chromium bound on the biomass was mostly or totally in trivalent form. These results were confirmed by XANES experiments. EXAFS spectroscopy demonstrates that the coordination environment of the chromium bounded at the surface of the biomass corresponds to Cr (III) in an octahedral geometrical arrangement. EPR spectra of Cr-laden soy hull biomass showed the presence of the intermediate oxo-Cr(V)-biomass at short contact time and only a signal corresponding to Cr(III) at long contact times, confirming the total reduction of Cr(VI) to Cr(III)-laden biomass. These spectroscopic evidences confirmed a proposed mechanism in which Cr(VI) is reduced to Cr(V) and finally to Cr(III). The reduced Cr(III) remained in the aqueous phase or bounded to the soy hull surface. Reduction rate of Cr(VI) is a process strongly related to temperature.

Two mathematical models (Thomas and modified dose–response) were employed to interpret the experimental breakthrough curves. The critical bed depth, Z_0 was 0.2 cm.

Soy hull biomass is a potential sorption agent for the reduction and removal of Cr(VI) from aqueous solutions. It has a better value of q_m compared with sorbents derived from minerals such as polyphenol-SiO_2, iron oxide membrane, and copper coated polymer foam. The high value of q_m and the low cost of this sorbent makes this new sorbent a better choice for continuous treatment of effluents polluted with chromate ions.

Acknowledgements

We thank the National Research Council of Argentina (CONICET)PIP 0037, National University of Rosario (UNR)PIP BIO259. We are indebted to Prof. Julio Ferron (Intec-Conicet) for the XPS measurements; Masafumi Harada (Faculty of Human Energy Accelerator Research Organization (KEK), Tsukuba, Japan) for the XAS measurements. We also thanks to Argentine Technological Founding of Environmental and Social Development, for equipment donation. PhD. Patricia Blanes thanks to National Academy of Physic, Exact and Natural Sciences for granting a PhD fellowship.

Appendix A. Supplementary data

Supplementary data associated with this article can be found, in the online version, at http://dx.doi.org/10.1016/j.jece.2015.12.008.

References

[1] R. Yu, F. Chi, W. Cheng, J. Chang, Chem. Eng. J. 255 (2014) 568–576.
[2] http://water.epa.gov/drink/contaminants/basicinformation/chromium.cfm.
[3] Y. Ma, W. Liu, N. Zhang, Y. Li, H. Jiang, G. Sheng, Biores. Technol. 169 (2014) 403–408.
[4] L. Alvarado, I.R. Torres, A. Chen, Sep. Purif. Technol. 105 (2013) 55–62.
[5] T.S. Kassem, Desalination 258 (2010) 206–218.
[6] D. Mohan, C.U. Pittman Jr., J. Hazard. Mater. 137 (2006) 762–811.
[7] A.S.K. Kumar, R. Ramachandran, S. Kalidhasan, V. Rajesh, N. Rajesh, Chem. Eng. J. 211–212 (2012) 396–405.
[8] Y. Cengeloglu, A. Tor, E. Kir, M. Ersoz, Desalination 154 (2003) 239–246.
[9] G. Almaguer-Busso, G. Velasco-Martinez, G. Carreno-Aguilera, S. Gutierrez-Granados, E. Torres-Reyes, A. Alatorre-Ordaz, Electrochem. Commun. 11 (2009) 1097–1100.
[10] B. Volesky, Water Res. 41 (2007) 4017–4029.
[11] B. Nasernejad, T. Esslam Zadeh, B. Bonakdar Pour, M. Esmaail Bygi, A. Zamani, Process Biochem. 40 (2005) 1319–1322.
[12] K. Chojnacka, J. Hazard, Mater. 121 (2005) 167–217.
[13] H. Parab, S. Joshi, N. Shenoy, A. Lali, U.S. Sarma, M. Sudersanan, Process Biochem. 41 (2006) 609–615.
[14] S. Bellú, L. Sala, J. González, S. García, M. Frascaroli, P. Blanes, J. García, J.M. Salas Peregrin, A. Atria, J. Ferrón, M. Harada, C. Cong, Y. Niwa, J. Water Res. Protect. 2 (2010) 888–897.
[15] S. Gupta, B.V. Babu, Chem. Eng. J. 150 (2009) 352–365.
[16] U. Maheshwari, S. Gupta, Res. J. Chem. Environ. 15 (2011) 939–943.
[17] A. Alemdar, M. Sain, Bioresour. Technol. 99 (2008) 1664–1671.
[18] W.P.F. Neto, H.A. Silverio, N. Oliveira Dantas, D. Pasquini, Ind. Crops Prod. 42 (2013) 480–488.
[19] R. Gnanasambandam, A. Proctor, Food Chem. 65 (1999) 461–467.
[20] M. Krumpolc, J. Roček, G.P. Haight Jr., P. Merrill, Inorg. Synth. 20 (1980) 63–65.
[21] H. Šillerova, M. Komarek, V. Chrastny, M. Novak, A. Vanek, O. Drabek, J. Colloid Interface Sci. 396 (2013) 227–233.
[22] M.A. Bezerra, R.E.E. Santelli, P. Oliveira, L.S. Villar, L.A. Esclaleira, Talanta 76 (2008) 965–977.
[23] J. Zolgharnein, A. Shahmoradi, J. Chem. Eng. Data 55 (2010) 5040–5049.
[24] C. Huang, L. Chen, H. Yang, M. Li, T. Pan, J. Hazard. Mater. 241–242 (2012) 190–196.
[25] L.S. Clesceri, A.E. Greenberg, Standard Methods of the Examination of Water and Wastewater, 20th ed., American Public Environment Federation, Washington, 1998, pp. 366–368.
[26] H.C. Thomas, J. Am. Chem. Soc. 66 (1944) 1664–1666.
[27] G. Yan, T. Viraraghavan, M. Chen, Adsorpt. Sci. Technol. 19 (2001) 25–43.
[28] M. Nomura, A. Koyama, Nucl. Instrum. Methods Phys. Res. A 467–468 (2001) 733–736.
[29] K.K. Kannan, M.A. Viswamitra, Acta Crystallogr.a 19 (1965) 151–152.
[30] C. Namasivayam, I.R. Kavitha, Microchem. J. 82 (2006) 43–48.
[31] C. Bouchelta, M.S. Medjram, O. Bertrand, J.P. Bellat, J. Anal. Appl. Pyrolysis 82 (2008) 70–77.
[32] H. Arslanoglu, H.S. Altundogan, F. Tumen, Biores. Technol. 99 (2008) 2699–2705.
[33] A. Sari, D. Mendil, M. Tuzen, M. Soylak, Chem. Eng. J 144 (2008) 1–9.
[34] V. Murphy, S. Tofail, H. Hughes, P. McLoughlin, Chem. Eng. J 148 (2009) 425–433.
[35] http://www.kemi.kth.se/medusa. Medusa Program (Make Equilibrium Diagrams Using Sophisticated Algorithms, version 18 November 2008). Ignasi Puigdomenech, Inorganic Chemistry, Royal Institute of Technology (KTH), SE-100 44 Stockholm, Sweden. (accessed April 2011).
[36] M. Gorgievski, D. Bozíc, V. Stankovíc, N. Strbac, S. Serbula, Ecol. Eng 58 (2013) 113–122.
[37] D. Park, S. Lim, Y. Yun, J.M. Park, Chemosphere 70 (2007) 298–305.
[38] D. Park, Y.S. Yun, C.K. Ahn, J.M. Park, Chemosphere 66 (2007) 939–946.
[39] I.M. Dittert, H. de Lima Brandão, F. Pina, E.A.B. da Silva, E.A.A.U. de Souza, S.M.A. G.U. de Souza, C.M.S. Botelho, R.A.R. Boaventura, V.J.P. Vilar, Chem. Eng. J. 237 (2014) 443–454.
[40] J.H. Espenson, Chemical Kinetcis and Reactions Mechanism, 2nd ed., McGraw Hill, New York, 2002.
[41] D. Park, Y.S. Yun, H.W. Lee, J.M. Park, Biores. Technol. 99 (2008) 1141–1147.
[42] D. Park, Y. Yun, J.Y. Kim, J.M. Park, Chem. Eng. J 136 (2008) 173–179.
[43] W.J. Weber, J.C. Morris, J. Sanit. Eng. Div. ASCE 89 (1963) 31–59.
[44] I. Langmuir, J. Am. Chem. Soc. 40 (9) (1918) 1361–1403.
[45] T.W. Weber, R.K. Chakravorti, J. Am. Inst. Chem. Eng. 20 (1974) 228–238.
[46] H.M.F. Freundlich, Z. Phys, Chem. 57 (1906) 385–470.
[47] M.M. Dubinin, L.V. Radushkevich, Proc. Acad. Sci. U.S.S.R. Phys. Chem. Sect. 55 (1947) 331.
[48] S.S. Dubey, R.K. Gupta, Sep. Purif. Technol. 41 (2005) 21–28.
[49] G. Bayramoglu, M.Y. Arica, Chem. Engin. J. 139 (2008) 20–28.
[50] V.C. Srivastava, I.D. Mall, I.M. Mishra, Chem. Engin. J. 132 (2007) 267–278.
[51] A. Kilislioglu, B. Bilgin, Appl. Radiat. Isotopes 50 (2003) 155–160.
[52] O.J. Redlich, D.L. Peterson, J. Phys. Chem. 63 (1959) 1024–1026.
[53] R. Sips, J. Chem. Phys. 16 (1948) 490–495.
[54] U. Maheshwari, S. Gupta, Adsorpt. Sci. Technol. 33 (2015) 71–88.
[55] M.L. Paul, J. Samuel, N. Chandrasekaran, A. Mukherjee, Chem. Engin. J. 187 (2012) 104–113.
[56] A.B. Albadarin, C. Mangwandi, G.M. Walker, S.J. Allen, M.N.M. Ahmad, M. Khraisheh, J. Environ. Manag. 114 (2013) 190–201.
[57] G.J. Copello, M.P. Pesenti, M. Raineri, A.M. Mebert, L.L. Piehl, E. Rubin de Celis, L. E. Diaz, Colloid Surf. B Biointerfaces 102 (2013) 218–226.
[58] M. Shi, Z. Li, Y. Yuan, T. Yue, J. Wang, R. Li, J. Chen, Chem. Engin. J 265 (2015) 84–92.
[59] A. Adamczuk, D. Kołodynska, Chem. Engin. J 274 (2015) 200–212.
[60] C. Li, Z. Du, W. Zou, H. Li, C. Zhang, React. Funct. Polym. 88 (2015) 24–30.
[61] V. Gopalakannan, N. Viswanathan, Int. J. Biol. Macromol. 72 (2015) 862–867.
[62] S. Chen, Q. Yue, B. Gao, Q. Li, X. Xu, Chem. Engin. J 168 (2011) 909–917.
[63] E. Malkoc, Y. Nuhoglu, Sep. and Purif. Technol. 54 (2007) 291–298.
[64] P. Suksabye, P. Thiravetyan, J. Environ. Manage. 102 (2012) 1–8.
[65] A. Albadarin, C. Mangwandi, G. Walker, S. Allen, M. Ahmad, M. Khraisheh, J. Environ. Manage. 114 (2013) 190–201.
[66] Y. Liu, Y.J. Liu, Sep. Purif. Technol. 61 (2008) 229–242.
[67] R.M. Schneider, C.F. Cavalin, M.A. Barros, C.R. Tavares, Chem. Engin. J. 132 (2007) 355–362.
[68] S. Sircar, R. Mohr, C. Ristic, M.B. Rao, J. Phys. Chem. B 103 (1999) 6539–6546.
[69] S. Sircar, Appl. Surf. Sci. 252 (2005) 647–653.
[70] M.R. Unnithan, T.S. Anirudhan, Ind. Eng. Chem. Res. 40 (2001) 2693–2701.
[71] D. Duranoglu, A.W. Trochimczuk, U. Beker, Chem. Engin. J. 187 (2012) 193–202.
[72] S. Chowdhury, R. Mishra, P. Saha, P. Kushwaha, Desalination 265 (2011) 159–168.
[73] S. Chowdhury, P. Saha, Colloid Surf. B Biointerfaces 88 (2011) 697–705.
[74] D. Park, Y.S. Yun, J.H. Jo, J.M. Park, Water Res. 39 (2005) 533–540.
[75] G. Barr-David, M. Charara, R. Codd, R.P. Farell, J.A. Irwin, P.A. Lay, R. Ramley, S. Brumby, J.I. Ji, G.R. Hanson, J. Chem. Soc. Faraday Transact. 91 (1995) 1207–1216.
[76] J.L. Gardea-Torresdey, K.J. Tiemann, V. Armendariz, L. Bess-Oberto, R.R. Chianelli, J. Rios, J.G. Parsons, G. Gamez, J. Hazard. Mater. 80 (2000) 175–188.
[77] R.S. Vieira, E. Meneghetti, P. Baroni, E. Guibal, V.M. Gonzalez de la Cruz, A. Caballero, E. Rodriguez-Castellon, M.M. Beppu, Mater. Chem. Phys. 146 (2014) 412–417.
[78] M.K. Kim, K.S. Sundaram, G.A. Iyengar, K.P. Lee, Chem. Eng. J. 267 (2015) (2015) 51–64.
[79] A.B. Albadarin, C. Mangwandi, A.H. Al-Muhtaseb, G.M. Walker, S.J. Allen, M.N. M. Ahmad, Chin. J. Chem. Eng. 20 (2012) 469–477.
[80] G.S. Bohart, E.Q. Adams, J. Chem. Soc. 42 (1920) 523–529.